FIELD TESTING OF NICKEL CONTAMINATED SEDIMENTS: NICKEL FLUX, CHEMICAL SPECIATION, AND TOXICITY TO AQUATIC INVERTEBRATES

David M. Costello[1]*, G. Allen Burton[1], Chad R. Hammerschmidt[2],

Anthony S. Honick[1], and Kevin W. Custer[2]

[1] University of Michigan

School of Natural Resources and Environment

440 Church St.

Ann Arbor, MI 48109, USA

[2] Wright State University

Department of Earth & Environmental Sciences

3640 Colonel Glenn Hwy.

Dayton, OH 45435, USA

* Corresponding author:

dcostel@umich.edu

(734)763-3602

Contents

1. Executive summary

In sediments, the pool of bioavailable metals is often much smaller than the total metals concentration due to complexation primarily with acid volatile sulfides (AVS), organic carbon (OC), and iron and manganese oxides (FeO_X and MnO_X). For nickel (Ni), these relationships have been demonstrated in the laboratory but rarely in lotic sediments under field conditions. In this study, five sediments with a range of inferred binding capacities (i.e., AVS and OC) were amended with Ni and deployed in the field for eight weeks. These five sediments, spiked in an identical manner with similar Ni concentrations, were used in parallel laboratory and acute toxicity assays. Three freshwater sediments (from Raisin River, St. Joseph River, and Spring River) were deployed in their stream of origin and sediment from Dow Creek, Mill Creek, and Spring River were deployed in Little Molasses Creek. Little Molasses Creek was selected for deployment of multiple sediments due to low water hardness and thus high overlying water Ni bioavailability. For each sediment, four Ni treatments were deployed (a control plus three increasing Ni concentrations) that covered a concentration range from presumably non-toxic to highly toxic. Ni-amended sediments were prepared using a "superspike" method with a long equilibration time (8 weeks) that created contaminated sediments more relevant to field conditions. At deployment and after four and eight weeks of incubation, surface and deep sediments were sampled to measure a suite physicochemical variables thought to influence Ni bioavailability. Also at deployment, caged *Hyalella azteca* were placed against the sediments and in the overlying water to monitor acute toxicity. At week 4 and 8, colonization baskets containing Ni-amended sediments were removed and all benthic macroinvertebrates were identified to family and enumerated. The colonizing benthic community was best described by six benthic indices: taxa richness, total abundance, Shannon diversity, Gammaridae abundance, Chironomidae abundance, and Ephemeroptera, Plecoptera, and Trichoptera (EPT) abundance. Diffusive gradients in thin films (DGTs) were placed in the sediments for 24-hours at all sampling periods to estimate Ni flux. Response variables (benthic indices and Ni flux) were predicted by sediment physicochemical variables with stepwise multiple linear regression followed by Akaike's Information Criterion (AIC), which compared models and selected the best model(s) based on fit and parsimony. Ni within the sediments changed dramatically through time and largely as a result of changes in partitioning. Although the pool of total Ni declined only marginally through time (median 13% decline from day 0 at week 8) Ni flux measured by DGTs declined 20x by week 8. Ni partitioning, estimated as the distribution coefficient (K_d), indicated that solid-phase Ni was bound initially to OC but through time shifted to associations with FeO_X and MnO_X. Although the flux of Ni was greatest at deployment, the caged *H. azteca* placed on the sediments experienced no acute toxicity. However, at week 4, five of the six benthic indices declined with increasing Ni bioavailability in the sediment. All the responding benthic indices exhibited an inverse relationship with simultaneously extracted Ni (SEM_{Ni}) whereas benthic indices were weakly related to total Ni and porewater Ni . For four of the five responding benthic indices, the addition of a parameter for AVS improved the model, whereas variables for OC and FeO_X+MnO_X improved models for only one and three of the benthic indices, respectively. At week 8, although total Ni and SEM_{Ni} declined minimally, only 2 of 6 benthic indices responded to any measure of Ni, with total abundance being the only index with a strong response to Ni. We suggest that Fe and Mn oxide formation is the primary driver of reduced Ni bioavailability at week 8. These results suggest that Ni diagenesis follows a predictable pattern of complexation with ligands (OC → AVS →

MnO_X) in freshwater lotic sediments, and diagenetically weathered deposits of Ni are less bioavailable. Additionally, the AVS-SEM model of bioavailability is applicable to Ni in freshwater sediments and outperforms measures of total Ni, porewater Ni, and Ni flux estimated from DGTs.

2. Introduction

Like other divalent metals, Ni is dynamic in sediments with bioavailability altered by flux, sorption, and partitioning processes. Physicochemical properties of sediments have critical control over the bioavailability of Ni; complexation of free Ni (Ni^{2+}) with organic ligands, acid volatile sulfides (AVS), and iron and manganese oxides (FeO_X and MnO_X) can reduce toxicity. Negatively charged functional groups in particulate and dissolved organic matter can complex Ni^{2+} but decomposition of particulate organic matter in sediment can mobilize Ni^{2+}, as either a dissolved complex or free ion, to porewater and overlying water (*1, 2*). Sulfur-reducing bacteria in anoxic sediments produce sulfides that precipitate Fe^{2+} and other divalent metals for which sulfide has a high affinity (i.e., Ni, Cu, Cd, Zn, Pb, Hg). These metal-sulfide precipitates are presumed to be unavailable to benthic organisms (*3, 4*). Mn and Fe oxides, which can be present in freshwater sediments at high concentrations, also can scavenge divalent metals and make them unavailable to biota (*5-7*).

Most of the recent research on Ni availability in sediments has focused on AVS and organic carbon (OC) as the primary ligands that form insoluble and non-toxic metal complexes. Empirical studies have found that mathematical combinations of simultaneously extracted nickel (SEM_{Ni}), AVS, and OC predict Ni toxicity better than total Ni concentrations (*3, 4, 6, 8-11*). Two theoretical metal availability criteria, calculated as the molar difference and ratio of SEM metals to AVS (SEM_{Me}-AVS and SEM_{Me}/AVS, respectively), identify thresholds where if AVS exceeds SEM (i.e., SEM_{Me}-AVS < 0 μmol g^{-1} and SEM_{Me}/AVS < 1) all of the metal should be as an insoluble metal sulfide and non-toxic. A third measure accounts for metal binding with OC (i.e., SEM_{Me}-AVS/fOC) and identifies non-toxic sediments as those with SEM_{Me}-AVS/fOC < 120 μmol g^{-1}. Studies of the applicability of these benchmarks for Ni contaminated sediments have been primarily conducted in laboratory settings (*3, 8, 9,* but see *11*); this study tests the utility of SEM-AVS models under field conditions.

The objective of this study is to test AVS-SEM models of bioavailability for Ni in freshwater sediments. Five sediments covering a range of binding capacity (i.e., AVS and OC content) were amended with Ni, deployed in the field under ambient conditions, and monitored for 8 weeks. Field-based manipulations allows for a controlled and replicated experiment while avoiding some artifacts of laboratory-based studies (e.g., elevated levels of Ni in overlying water, unrealistic flow conditions). This study is an improvement over previous Ni bioavailability field experiments due to (1) novel sediment treatment methods that produce more realistic Ni distribution between solid and dissolved phases and minimized diffusional loss, (2) more sediments with greater combinations of potential binding agents, (3) experiments in lotic ecosystems, which provide a more robust test of SEM-AVS theory, and (4) a paired lab experiment with the same sediments for comparison of results. Stream chemistry, sediment physicochemistry, and Ni partitioning and flux were measured to model the response of caged organisms and the colonizing benthic macroinvertebrate community to sediment Ni. Our hypothesis was that SEM_{Ni}-AVS/fOC would best predict the response of the benthic community.

3. Methods

3.1. Sediment selection

A synoptic survey of AVS and OC in stream sediments in Michigan and Missouri was conducted to select sediments with a range of AVS and OC and inferred Ni binding capacity. Five sediments were selected for use: Spring was predicted to have the lowest binding capacity (low AVS and OC) whereas Mill had the highest (high AVS and OC) with Raisin, Dow, and St. Joseph having intermediate binding capacities (Table 1). To collect sediments for amendment with Ni we returned to each location and removed ~75 L of sediment with shovels and placed it into plastic bags within buckets, sealed with little headspace, and kept cool (4°C).

3.2. Ni-treated sediments

All sediments were amended with Ni by a "superspike" method that was used to minimize losses of AVS and changes in pH (similar to Hutchins et al. [*12*]). For the superspike method, a small volume of each sediment was amended with $NiCl_2$, equilibrated, and then diluted with untreated sediment to achieve the desired concentrations. The pH of initial superspike sediments was adjusted with NaOH and allowed to equilibrate for 4 weeks with weekly 1-hr rolling. To avoid loss of AVS, any added water was deoxygenated and the headspace of all jars was filled with N_2 gas whenever opened. After the 4 week equilibration, superspike sediments were diluted with corresponding untreated sediments to achieve three concentrations of Ni (i.e., Low, Medium, High). Target Ni concentrations (57-6574 mg/kg dry) were related to predicted binding capacity for each sediment type with higher binding sediments (e.g., Mill) amended with relatively greater amounts of Ni than lower binding sediments (e.g., Spring) (Table 1). Sediments at the target Ni concentrations were equilibrated for an additional 4 weeks by rolling weekly prior to deployment in the field.

3.3. Site selection

Ni-amended sediments were deployed in three streams in Michigan and one in Missouri (Table 2). Spring, Raisin, and St. Joseph sediments were redeployed in their respective streams. Mill, Dow, and a second set of Spring sediments were deployed in Little Molasses Creek. Little Molasses Creek was selected for deployment of multiple sediment types because of its relatively low water hardness, which is known to increase the bioavailability of divalent metals (*13, 14*). During sediment deployment, water temperature, pH, dissolved O_2, specific conductance, and turbidity were measured continuously at each site with sondes. Water hardness and alkalinity were measured three times during the deployment.

3.4. Sediment deployment

Sediments were deployed in colonization trays or toxicity trays in August of 2009 during baseflow conditions. Colonization trays consisted of plastic baskets (25 x 7 x 6 cm) lined with 1-mm mesh, which were attached in triplicate to epoxy-coated wire shelving and encased in mesh nylon bags (Figure 1A). For each sediment-treatment combination, six colonization baskets were used with three each removed after 4 and 8 weeks of deployment. Toxicity trays consisted of a plastic-coated wire tray (33 x 26 x 6 cm) lined with 1-mm mesh encased in mesh nylon bags. Mesh nylon bags were used to reduce the loss of

sediment during storm events yet the mesh size (5 mm) was large enough to allow most macroinvertebrates to colonize the trays (*10*). All trays were placed on the steam bottom flush with the existing sediment and secured with rebar. Trays were placed in the stream according to Ni treatment with reference sediments upstream of Ni treatments that increased in order downstream.

3.5. In situ *acute toxicity*

After deploying the sediments in the stream, *in situ* chambers containing *Hyalella azteca* were placed on the toxicity trays for four days to assess acute toxicity. *In situ* chambers were cellulose acetate butyrate cylinders (7 cm diameter) with 80-µm mesh windows (*10*) containing 10 *H. azteca* and ~30 mg dry weight (dw) of microbial-conditioned, 1 cm diameter leaf disks (*Acer rubrum*). Six chambers were filled with site water and placed on each sediment-treatment combination with three chambers exposed to the sediment (mesh windows down) and three exposed to the overlying water (mesh windows to the side). The chambers were secured to the toxicity tray with epoxy-coated wire shelving and cable ties (Figure 1B). After four days, the chambers were removed, *H. azteca* were counted, and leaf disks were recovered, rinsed, and dried. Dried leaf disks were reweighed and the weight loss was used to estimate *H. azteca* feeding rates. Due to limited observed acute effects immediately after deploying the sediments, the *in situ* acute toxicity assays were not conducted during later stages of the test.

3.6. Diffusive gradients in thin films (DGTs)

One DGT was placed in each sediment-treatment combination to estimate the flux of Ni, Mn, and Fe from sediments. DGTs loaded within plastic spikes were pushed into and through designated colonization baskets to a mark for the sediment water interface. After ~24 hours, the DGTs were carefully removed from the baskets, rinsed with Milli-Q water, and placed in a plastic bag and stored refrigerated. Each DGT was carefully sectioned with a Teflon-coated razor blade into three portions: 2 cm from just above the sediment-water interface that was exposed to the water column (WC), 1 cm from just below the sediment-water interface (TOP), and a 1-cm section from deeper in the sediment (between 2-3 cm) (BOT). Each section was placed in an acid-cleaned centrifuge tube and extracted with 1 mL of 1 M nitric acid. The extract from each DGT was analyzed for Ni and Mn with inductively coupled plasma mass spectrometery (ICP-MS) and Fe determined by flame atomic adsorption spectrometery (FAAS). Due to fluctuating and often increased turbidity and water depth in Spring River, DGTs could not reliably be deployed and recovered there and the data presented is from the three Michigan streams.

3.7. Sediment colonization and geochemistry

After 4 and 8 weeks of deployement, sediment colonization trays were recovered from the streams and sampled. Results for trays deployed in Spring River are limited to week 4 only, as a result of a massive flood at week 6 that buried all of the trays under natural sediment. At each sampling time, three colonization trays from each sediment-treatment combination were sampled. From those trays, one third of each tray was combined and homogenized for geochemistry analysis while the remaining two-thirds of each tray was placed into a separate 1-L LDPE bottle with 90% ethanol for assessment of the benthic macroinvertebrate community. Sediment samples reserved for assessment of the colonizing macroinvertebrate community were sieved (45 µm) and all macroinvertebrates were removed,

identified to the family level (*15*), and enumerated. The colonizing benthic community was described by six indices: taxa richness (family level), abundance, Shannon diversity, Chironomidae abundance, Gammaridae abundance, and Ephemeroptera, Plecoptera, and Trichoptera (EPT) abundance.

Sediment reserved for geochemical analyses was further subdivided into surface (0-2 cm) and deep (2-6 cm) sediment. Surface and deep sediments were preserved by freezing for analysis of AVS, SEM_{Me} (Ni, Mn, and Fe), % solids, wet density, OC , $CaCO_3$. Remaining surface and deep sediment was combined and refrigerated for analysis of porewater Ni, total metals (Ni, Fe, Mn), and dissolved organic carbon (DOC). Standard gravimetric techniques were used to measure organic content (loss-on-ignition at 550°C for > 1 h), carbonate content (1000°C heating of remaining material for > 1 h), and density of lyophilized sediments (*16*). Loss-on-ignition was converted to OC using the Redfield ratio of C in organic matter (0.36) (*17*). AVS and SEM_{Me} were measured using the methods and apparati described by Allen et al. (*18*), which involves the acidification of sediment followed by capture of H_2S in NaOH traps. Sulfide was determined colorimetrically with mixed diamine reagent (*18*) and SEM_{Me} was measured by FAAS after filtration. If SEM_{Me} concentrations were below detection limit of FAAS, samples were analyzed using ICP-MS. Fe and Mn oxides (FeO_X+MnO_X) were estimated as the 1 N HCl extracted Fe and Mn in excess of AVS ([SEM_{Mn} + SEM_{Fe}] – AVS). For porewater Ni and DOC, sediments were centrifuged, supernatant filtered through 0.45-µm polycarbonate membrane, and filtrate analyzed with ICP-MS and a OC analyzer (Teledyne Tekmar Apollo 9000), respectively. Total metals were determined by FAAS after microwave digestion of sediment in concentrated nitric acid

3.8. Statistical analysis

All statistical analyses were conducted using R 2.8.1 (*19*). *In situ* survival and feeding of *H. azteca* were analyzed with separate one-way ANOVAs for each sediment type and exposure compartment (overlying water vs. sediment). To meet the assumptions of ANOVA, all survival data were arcsine square root transformed and feeding rates were square root transformed when variances were unequal. The design of the experiment (multiple sediment types with few treatment levels) allowed for the benthic data to be analyzed used regression techniques. Due to the complexities of field experiments (including limited replication and highly variable controls), it is difficult and impractical to perform ANOVAs for particular sediment types (i.e., calculate no observed effect concentrations). However, by grouping multiple sediments in a single regression analysis, the power of the statistical test is greatly improved and it is possible to find unified relationships that are applicable to a wide variety of field conditions.

The partitioning of Ni between porewater and solid phases was examined by calculating a Ni partitioning coefficient (K_d):

$$K_d\left(\mathrm{L\ kg^{-1}}\right) = \frac{\text{solid Ni } (\mu\text{mol kg}^{-1})}{\text{porewater Ni } (\mu\text{mol L}^{-1})}$$

Greater K_d values indicate relatively more Ni bound to the solid phase and low values signify proportionately more Ni in the porewater. Log K_d was compared among sampling dates using one-way ANOVA, followed by a Tukey HSD post hoc test. At each sampling date, multiple linear regression was used to predict log K_d from measured physicochemical parameters in surface and deep sediments (i.e.,

total Fe, total Mn, SEM_{Mn}, SEM_{Fe}, FeO_X+MnO_X, OC, AVS, $CaCO_3$, and density). All explanatory variables were log transformed. Stepwise selection was used to determine parameter inclusion and Akaike's Information Criterion with sample size correction (AICc) was used for selection of the "best" model(s) for Ni K_d at each sampling date. AICc compares models both based on fit (i.e., likelihood) and parsimony with the lowest AICc value assigned to the model with the best fit with the least number of predictor variables (*20*). For stepwise selection, the parameter that increased the model fit (i.e., increased log likelihood) by the greatest amount was added first and additional parameters were added individually until the likelihood was maximized. Due to potential multicollinearity between our predictor variables, at each step any potential variable with a variance inflation factor (VIF) >2 was removed from the list of potential parameters (*21*). For each model produced during the stepwise procedure, an AICc value was calculated and those models within 2 of the minimum AICc value were considered to be potential "best" models.

The colonizing macroinvertebrate community indices also were analyzed with stepwise multiple linear regression with AICc. Potential explanatory variables for our benthic community indices included: all the measures of Ni bioavailability in surface and deep sediments (total Ni, porewater Ni, SEM_{Ni}, SEM_{Ni}/AVS, SEM_{Ni}-AVS, SEM_{Ni}-AVS/fOC, and K_d), and additional sediment physicochemical parameters (AVS, OC, total Fe, total Mn, SEM_{Fe}, SEM_{Mn}, FeO_X+MnO_X, $CaCO_3$, and density). When statistically significant, a blocking factor for stream was added to the model to account for differences in the resident benthic community available to colonize the baskets. All predictor variables were log transformed except for SEM_{Ni}-AVS and SEM_{Ni}-AVS/fOC, which were log + 1 transformed after negative values, which are predicted to be non-toxic (*4, 10*), were converted to 0. Stepwise and AICc procedures for benthic indices were completed as noted above. A dose-response curve for Gammaridae, which was the most sensitive benthic index, was produced using binomial logistic regression.

Ni fluxes measured with DGTs at different levels in the sediment were analyzed with the same stepwise and AICc procedure used for the benthic indices. All flux measurements were log transformed to reduce the influence of outliers. Additionally, correlation between benthic indices and DGT fluxes measured at week 4 were analyzed using Pearson's product-moment coefficient.

4. Results and discussion

4.1. Ni-treated sediments

At deployment, the binding capacity (i.e., AVS and OC) of most Ni-amended sediments was similar to that measured in the synoptic sediment survey; however, Raisin sediment had lower OC and Mill had lower AVS than measured in the survey (Table 3). Measured concentrations of Ni were 5-50% less than nominal in all sediments with the exception of Raisin sediments, which were 70-80% lower than nominal concentrations. The deviations from target Ni concentrations were due to errors in the density to solid ratio estimates used during the superspike preparation and dilutions. The relative differences between the three Ni-amended treatments for each sediment type were similar to the relative differences of nominal concentrations. Although Ni concentrations were less than expected, each sediment type had at least 2 treatments at day 0 with Ni concentrations great enough to exceed non-toxic benchmarks (SEM_{Ni}-AVS > 0 μmol g^{-1}, SEM_{Ni}/AVS >1, and SEM_{Ni}-AVS/fOC > 120 μmol g^{-1}).

4.2. In situ *acute toxicity*

Although amphipods are very sensitive to Ni (*22*), no significant mortality was observed for *H. azteca* placed on the sediment or in the water column for any Ni-amended sediments (Table 4). Reduced survival, though only marginally significant, was observed on Spring sediments deployed in Spring River and Dow sediments. *H. azteca* on Spring sediments in Spring River showed declines in survival at medium and high Ni concentrations (40 and 47%, respectively) relative to reference and low sediments (93 and 97%, respectively). Marginally significant mortality was observed on Dow sediments due to reduced *H. azteca* survival on reference sediments. Reduced *H. azteca* survival on Spring sediments, which had one of the lowest binding capacities, was not unexpected, yet the Spring sediments placed in Little Molasses Creek exhibited no acute toxicity. Little Molasses Creek was more turbid than Spring River (Table 1) and the elevated suspended solids may have been protective by sorbing the Ni fluxing from the sediment (*23*).

For sublethal effects, we observed no change in *H. azteca* feeding rates on leaf disks for organisms exposed to overlying water; however, for *H. azteca* exposed to the sediment surface, we observed a significant increase in feeding rates with increasing Ni concentrations on Raisin sediment. There was no measured change in the feeding rate of *H. azteca* exposed to the sediment surface of all other sediments. Collectively, the absence of reduced feeding rates and the lack of significant mortality indicate that these Ni-amended sediments are not acutely toxic to caged benthic organisms. However, these sediments do have the potential to negatively affect benthic organisms, and this was observed in the colonizing benthic macroinvertebrate community (see below).

4.3. DGTs

As expected, Ni flux was related positively to the sediment Ni concentrations (Figure 2). Ni flux changed considerably through time, with flux on day 0 ~3x higher than at week 4 and ~20x greater than the flux at week 8. The change in Ni flux was not due to a decline in Ni through time as total Ni concentrations at week 4 and 8 (median 92 and 87% of initial, respectively) were similar to those at deployment. Rather, the decline in Ni flux though time is presumably due to a change in the partitioning of Ni within the sediments; as Ni amendments to sediment age, the Ni shifts from labile forms to more recalcitrant fractions. The high treatment for Raisin sediments had a greater flux of Ni on day 0 and at week 4 than other all other sediments whereas the high treatment for St. Joseph sediments had the greatest flux rate of all sediments at week 8. In general, Ni flux was greatest from the deep sediment and water column Ni flux was always relatively low. The depth of the maximum Ni flux (2-3 cm) and the absence of a significant Ni flux in the water column is similar to what was observed in other Ni DGTs studies (*24, 25*).

Factors controlling Ni flux differed depending on the sediment compartment (i.e., water column, surface, and deep sediment) and changed through time. Ni flux on day 0 in the water column and surface sediment was related to sediment total Ni and in the deeper sediment porewater Ni and $CaCO_3$ (Tables 5, A1). At week 4, Ni fluxes in surface and deep sediment were both related to total Ni, AVS, and SEM_{Mn} in deep sediment, whereas Ni flux in the water column was only related to sediment total Ni (Tables 5, A2). The shift in physicochemical controls of Ni flux suggests that Ni binding changes through

time as the Ni-amended sediment aged in the streams. The flux measurements suggest that there is free Ni on day 0 and by week 4, the N flux is reduced by Ni bound to sulfides and manganese oxides. At week 8, Ni flux in the water column was not related to any measured sediment Ni variables but was related to sediment density and surface OC. In the sediment, Ni flux at the surface was related to total Ni and surface SEM_{Mn} while flux at depth was related to SEM_{Ni}-AVS/fOC (Tables 5, A3). Although DGTs are designed to measure the bioavailable Ni fraction, the models indicated that total Ni was the best predictor of flux. However, previous studies (*4, 10, 14, 26, 27*) and the benthic results (see below) indicate that total recoverable metal concentrations are almost certainly not the best measure of bioavailable metals.

Mn flux was not related to Ni treatments and did not differ substantially among sediment types (Figure 3). On day 0, Mn flux was greater in deep sediments but at week 4 and 8 surface and deep sediments were fluxing Mn at a similar rate. There was minimal flux of Mn to the water column with the exception of Spring sediment on day 0 and St. Joseph and Raisin sediments at week 4. In general, Fe flux was more variable among sediment treatments and through time than Mn flux. There was significant variation in Fe flux in the sediments on day 0; the sediment with the lowest binding capacity (Spring) had no measurable Fe flux, whereas the sediments with the highest binding capacity (Mill) had the greatest Fe flux (Figure 4). Fe flux was positively related to our Ni treatments only in Mill sediment on day 0, and this trend was stronger in the deeper sediment. For most sediment types, Fe flux declined through time. As expected, Fe flux was greater at depth and there was no measured Fe flux into the water column (*24*).

4.4. Ni partitioning (K_d)

Ni partitioning changed through time with a greater proportion of Ni in the porewater on day 0 and more Ni in the solid phase at week 4 and 8 ($F_{2,67} = 4.5$, $p = 0.01$). The increased proportion of porewater Ni at deployment is presumably due to the static Ni-amendments. The physicochemical variables controlling Ni K_d changed through time as the sediments went through diagenetic changes. At deployment, amended Ni was bound almost exclusively to sediment organic matter. On day 0, Ni K_d was predicted by OC, SEM_{Mn}, and $CaCO_3$ with OC being the primary driver of Ni partitioning (Figure 5A, Table A4). AIC indicated that a second model including just OC and SEM_{Mn} had a similar predictive power (Figure 5A, Table A4). At week 4, Ni had shifted from being bound to carbon to being bound to Fe. Ni K_d was related to total Fe (Figure 5B) and AIC indicated that models with additional parameters for AVS (deep) and OC (surface) offered only slight improvement in predictive power (Table A4). At week 8, Ni binding changed again and was now bound primarily to Fe and Mn oxides. Ni K_d was predicted by FeO_X+MnO_X and $CaCO_3$ and AIC indicated a second model including just FeO_X+MnO_X had similar predictive power (Figure 5C, Table A4). Although Ni binding changed through time, the slope of the K_d relationships did not differ among sediment types as each sediment followed the same diagenetic process. The sediment predictor variables strongly predicted Ni K_d on day 0 but these relationships became weaker (i.e., r^2 declined) through time (Table A4). Although proposed as the primary binding agent for divalent metals (*3, 6, 18*), AVS was not an important variable for predicting Ni K_d. The progression of Ni binding fractions as determined by K_d is much more informative than the relationships derived from DGT Ni fluxes.

4.5. Benthic colonization

The colonizing benthic macroinvertebrate community exhibited a strong response to the Ni-amendments 4 weeks after deployment with 5 out of 6 of the benthic indices negatively influenced by at least one measure of Ni in sediment (Table 6). Measures describing the entire benthic community (i.e., richness, abundance, and diversity) were best predicted by different parameters describing Ni bioavailability. Invertebrate abundance was best predicted by SEM_{Ni} whereas taxa richness was best predicted by AVS corrected Ni (i.e., SEM_{Ni}/AVS) and diversity by AVS and OC corrected Ni (i.e., SEM_{Ni}-AVS/fOC) (Table 6, A2). The relationship between richness and deep sediment SEM_{Ni}/AVS is linear (Figure 6) and there is no sharp decline in richness as SEM_{Ni}/AVS exceeds the proposed threshold above which toxicity may occur (SEM_{Ni}/AVS > 1) (*3, 4, 10*). Shannon diversity is reduced when SEM_{Ni}-AVS/fOC exceeds the proposed threshold of 100-150 µmol g^{-1} (*10*); however, Shannon diversity on Dow sediment (which was characterized as a low binding sediment) was reduced at a SEM_{Ni}-AVS/fOC below the threshold (31 µmol g^{-1}) (Figure 7). Individual colonizing taxa exhibited diverse responses to Ni at week 4. As expected, EPT taxa and Gammarus were very sensitive to Ni (*15, 22*) whereas Chironomids did not respond to Ni at the concentrations used in this study. Declines in EPT and Gammarus were best explained by SEM_{Ni} in deep sediment and Gammaridae colonization exhibited a strong dose-response relationship ($p < 0.001$) (Figure 8). Although the colonizing benthic community is responding to sediment Ni at week 4, there are no significant correlations between the Ni flux measured with DGTs and any of the benthic indices (Table 7). This indicates that for assessing Ni contaminated sediments, DGTs are not a sufficient surrogate for colonizing macroinvertebrates.

The AIC model selection suggests that Ni in deeper sediment and in the SEM fraction were most likely to negatively influence the macroinvertebrate community. For the five benthic indices that responded to Ni, four indices indicated an inverse relationship with Ni in deep sediment with only Shannon diversity responding to Ni in surface sediments (Table 6). Although laboratory studies have found Ni in surface sediments to cause toxicity (*8*), in this study it was observed that benthic invertebrates responded to deeper sediments. Invertebrates may be burrowing into these relatively fine sediments and interacting with the anoxic Ni-contaminated sediments. Alternatively, the DGT results indicated a significant amount of Ni flux at depth, and Ni in deeper sediments may have been a source for Ni in surficial sediments where it can impact surface invertebrates. Although total Ni was closely correlated to SEM_{Ni} (Pearson R = 0.80, $p < 0.001$), during model selection SEM_{Ni} always produced better models than total Ni. Moreover, although free Ni in porewater has been suggested as the likely toxic form of Ni (*4, 27*), SEM_{Ni} always outperformed direct measures of porewater Ni in predicting the benthic response. The small concentration differences between total Ni and the SEM fraction seem to be crucial to assessing Ni bioavailability to benthic organisms. These results suggest that measuring Ni concentrations after a cold acid extraction, even without measuring AVS or Mn, could greatly improve estimates of bioavailable Ni.

Although measures of Ni were the primary drivers of the measured benthic indices, multiple regression identified other sediment physicochemical variables that modified the benthic response. Models for Shannon diversity and EPT abundance were improved by the inclusion of AVS and models for taxa richness and Gammarus abundance were improved by including SEM_{Mn}. Together with modifications to Ni bioavailability (e.g., SEM_{Ni}/AVS), at least one measure of AVS was included in four of the five benthic

indices that had responded to Ni at week 4(Table 6). In comparison, variables for Mn were selected for two models and OC in just one model. Collectively, these models suggest that for colonizing benthic macroinvertebrates AVS is the most likely ligand reducing Ni bioavailability followed by Mn oxides then organic carbon.

For the second sampling period, the colonizing benthic macroinvertebrate community response to Ni changed significantly. Median total Ni and deep SEM_{Ni} declined minimally (10% and 3%, respectively) from week 4 to 8, yet for the most part, the benthic macroinvertebrates were not adversely affected by Ni. Of the six benthic indices measured, only two were inversely related to Ni (Table 6). Total abundance was best predicted by surface SEM_{Ni} and Chironomidae abundance included surface SEM_{Ni} as the tertiary variable in a three parameter model (Table 6, A3). Taxa richness, Shannon diversity, and EPT abundance were all related to sediment physicochemical variables other than Ni and Gammaridae abundance was not related to any of the measured sediment variables (Table 6, A3). The temporal trend in this study is in contrast to Nguyen et al. (*11*), who observed Ni toxicity 9 months after sediment deployment. In this study, Ni was distributed more realistically between porewater and solid phase and the lotic sediments had greater binding capacity (more representative of natural sediments), which may explain the temporal differences between the two studies.

The minimal response by the benthic community at week 8 in the presence of elevated total Ni concentrations indicates that the Ni is bound to ligands which make it unavailable to biota. Due to the increased influence of Mn and Fe oxides in the distribution of Ni at week 8, we suggest that Mn and Fe oxide surfaces may be binding Ni and reducing bioavailability (*5, 7*). Porewater (Table A7) and DGT (Figure 2) measurements from week 8 indicate that there is some free, mobile Ni at depth. However, as the sediments age in the field, the oxic surface sediments act as a "cap" which binds the Ni, and make the sediments non-toxic. Because we observed minimal toxicity, even at the highest Ni concentrations, the Fe and Mn oxide pool must be large enough to bind most of the available Ni. This result suggests that for lotic sediments with sufficient Fe and Mn, a Mn and Fe oxide corrected measure of Ni bioavailability may offer improved predictive power of Ni bioavailability.

4.6. Summary

The careful, detailed, and thorough analytical methods used in this study allowed for elucidations of trends between biogeochemistry and benthic macroinvertebrates that are representative of field conditions and can be used to create protective bioavailability models. Ni-amended sediments followed a predictable pattern of diagenesis after deployment in the streams with Ni initially bound to OC then switching to complexation with AVS and MnO_X. Similar to lab results (*3, 8, 9*), the SEM-AVS models did predict the invertebrate response with SEM_{Ni} as the bioavailable fraction and AVS binding to Ni and reducing toxicity. The protective effects of OC expected by the SEM-AVS models were rarely observed, but rather there was evidence that sorption to Fe and Mn oxides reduced the bioavailability of Ni. This suggests that future SEM-AVS models should explicitly include pools of FeO_X and MnO_X as potential metal ligands able to reduce toxicity. Surprisingly, direct measures of Ni flux with DGTs were poor predictors of Ni toxicity and were outperformed by the SEM-AVS models. Although this study did not definitively identify a single SEM-AVS model as superior, as a group, the SEM-AVS models did

outperform measures of total Ni, porewater Ni, and Ni flux and thus are the preferred method for estimating bioavailable Ni in freshwater sediments.

5. Literature cited

(1) Doig, L. E.; Liber, K., Nickel speciation in the presence of different sources and fractions of dissolved organic matter. *Ecotoxicology and Environmental Safety* **2007,** 66, 169-177.

(2) Shaw, T. J.; Gieskes, J. M.; Jahnke, R. A., Early diagenesis in differing depositional-environments - the response of transition-metals in pore water. *Geochimica Et Cosmochimica Acta* **1990,** 54, (5), 1233-1246.

(3) Di Toro, D. M.; Mahony, J. D.; Hansen, D. J.; Scott, K. J.; Carlson, A. R.; Ankley, G. T., Acid volatile sulfide predicts the acute toxicity of cadmium and nickel in sediments. *Environmental Science & Technology* **1992,** 26, (1), 96-101.

(4) Di Toro, D. M.; Mahony, J. D.; Hansen, D. J.; Scott, K. J.; Hicks, M. B.; Mayr, S. M.; Redmond, M. S., Toxicity of cadmium in sediments: the role of acid volatile sulfide. *Environmental Toxicology and Chemistry* **1990,** 9, (12), 1487-1502.

(5) Tebo, B. M.; Bargar, J. R.; Clement, B. G.; Dick, G. J.; Murray, K. J.; Parker, D.; Verity, R.; Webb, S. M., Biogenic manganese oxides: properties and mechanisms of formation. *Annual Review of Earth and Planetary Sciences* **2004,** 32, 287-328.

(6) Burton Jr., G. A.; Green, A.; Baudo, R.; Forbes, V.; Nguyen, L. T. H.; Janssen, C. R.; Kukkonen, J.; Leppanen, M.; Maltby, L.; Soares, A.; Kapo, K.; Smith, P.; Dunning, J., Characterizing sediment acid volatile sulfide concentrations in European streams. *Environmental Toxicology and Chemistry* **2007,** 26, (1), 1-12.

(7) Takematsu, N., Sorption of transition metals on manganese and iron oxides, and silicate minerals. *Journal of the Oceanographical Society of Japan* **1979,** 35, 36-42.

(8) Vandegehuchte, M. B.; Roman, Y. E.; Nguyen, L. T. H.; Janssen, C. R.; De Schamphelaere, K. A. C., Toxicological availability of nickel to the benthic oligochaete *Lumbriculus variegatus*. *Environment International* **2007,** 33, 736-742.

(9) Lee, J.-S.; Lee, J.-H., Influence of acid volatile sulfides and simultaneously extracted metals on the bioavailability and toxicity of a mixture of sediment-associated Cd, Ni, and Zn to polychaetes *Neanthes arenaceodentata*. *Science of the Total Environment* **2005,** 338, 229-241.

(10) Burton Jr., G. A.; Nguyen, L. T. H.; Janssen, C.; Baudo, R.; McWilliam, R. A.; Bossuyt, B.; Beltrami, M.; Green, A., Field validation of sediment zinc toxicity. *Environmental Toxicology and Chemistry* **2005,** 24, (3), 541-553.

(11) Nguyen, L. T. H.; Burton, G. A.; Schlekat, C. E.; Janssen, C. R., Field measurement of nickel sediment toxicity: role of acid volatile sulfide. *Environmental Toxicology and Chemistry* **In press**.

(12) Hutchins, C.; Teasdale, P.; Lee, S.; Simpson, S., The effect of sediment type and pH-adjustment on the porewater chemistry of copper- and zinc-spiked sediments. *Soil & Sediment Contamination* **2009,** 18, (1), 55-73.

(13) Nowierski, M.; Dixon, D. G.; Borgmann, U., Effects of water chemistry on the bioavailability of metals in sediment to *Hyalella azteca*: implications for sediment quality guidelines. *Archives of Environmental Contamination and Toxicology* **2005,** 49, 322-332.

(14) Pagenkopf, G. K., Gill surface interaction model for trace-metal toxicity to fishes: role of complexation, pH, and water hardness. *Environmental Science & Technology* **1983,** 17, (6), 342-347.

(15) Clements, W. H.; Carlisle, D. M.; Lazorchak, J. M.; Johnson, P. C., Heavy metals structure benthic communities in Colorado mountain streams. *Ecological Applications* **2000,** 10, (2), 626-638.

(16) Heori, O.; Lotter, A. F.; Lemcke, G., Loss on ignition as a method for estimating organic and carbonate content in sediments: reproducibility and comparability of results. *Journal of Paleolimnology* **2001,** 25, 101-110.
(17) Redfield, A. C., On the proportions of organic derivitives in sea water and their relation to the composition of plankton. In *James Johnstone Memorial Volume*, Daniel, R. J., Ed. Liverpool University Press: Liverpool, U.K., 1934; pp 176-192.
(18) Allen, H. E.; Fu, G.; Boothman, W.; DiToro, D. M.; Mahony, J. D. *Determination of acid volatile sulfide and selected simultaneously extractable metals in sediment*; USEPA: 1991; p 18.
(19) R Development Core Team *R: A language and environment for statistical computing*, R Foundation for Statistical Computing: Vienna, Austria, 2008.
(20) Burnham, K. P.; Anderson, D. R., Multimodel inference - understanding AIC and BIC in model selection. *Sociological Methods & Research* **2004,** 33, (2), 261-304.
(21) Graham, M. H., Confronting multicollinearity in ecological multiple regression. *Ecology* **2003,** 84, (11), 2809-2815.
(22) Milani, D.; Reynoldson, T. B.; Borgmann, U.; Kolasa, J., The relative sensitivity of four benthic invertebrates to metals in spiked-sediment exposures and application to contaminated field sediment. *Environmental Toxicology and Chemistry* **2003,** 22, (4), 845-854.
(23) Cloran, C. E.; Burton, G. A.; Hammerschmidt, C. R.; Taulbee, W. K.; Custer, K. W.; Bowman, K. L., Effects of suspended solids and dissolved organic carbon on nickel toxicity. *Environmental Toxicology and Chemistry* 29, (8), 1781-1787.
(24) Tankere-Muller, S.; Zhang, H.; Davison, W.; Finke, N.; Larsen, O.; Stahl, H.; Glud, R. N., Fine scale remobilisation of Fe, Mn, Co, Ni, Cu and Cd in contaminated marine sediment. *Marine Chemistry* **2007,** 106, 192-207.
(25) Zhang, H.; Davison, W.; Miller, S.; Tych, W., *In-situ* high-resolution measurements of fluxes of Ni, Cu, Fe, and Mn and concentrations of Zn and Cd in porewaters by DGT. *Geochimica Et Cosmochimica Acta* **1995,** 59, (20), 4181-4192.
(26) Borgmann, U.; Néron, R.; Norwood, W. P., Quantification of bioavailable nickel in sediments and toxic thresholds to *Hyalella azteca*. *Environmental Pollution* **2001,** 11, 189-198.
(27) Di Toro, D. M.; McGrath, J. A.; Hansen, D. J.; Berry, W. J.; Paquin, P. R.; Mathew, R.; Wu, K. B.; Santore, R. C., Predicting sediment metal toxicity using a sediment biotic ligand model: Methodology and initial application. *Environmental Toxicology and Chemistry* **2005,** 24, (10), 2410-2427.

Tables

Table 1. Mean (±1 SD) stream physical and chemical parameters recorded during the 8 week period (Aug. 2009-Oct. 2009) of Ni-amended sediment deployment. Temperature, dissolved O_2, specific conductance, and turbidity were measured every hour with a datasonde and hardness and alkalinity were measured three times during the experiment.

Stream	Latitude	Longitude	Temp. (°C)	pH	Dissolved O_2 (% sat.)	Specific conductance (µS cm^{-1})	Turbidity (NTU)	Hardness (mg L^{-1} $CaCO_3$)	Alkalinity (mg L^{-1} $CaCO_3$)
Spring R, MO[1]	37° 13.36'	94° 35.96'	19.0 ± 2.3	7.9 ± 0.26	78.4 ± 19	NA	30.6 ± 40.4	119 ± 30	93 ± 39
Raisin R., MI	42° 10.04'	84° 7.37'	15.7 ± 4.5	8.0 ± 0.13	88.0 ± 6.6	302 ± 21	28.6 ± 47.3	245 ± 11	216 ± 7
St. Joseph R., MI	42° 6.91'	84° 50.74'	14.8 ± 4.1	8.1 ± 0.16	91.0 ± 6.5	522 ± 28	67.0 ± 165	316 ± 10	242 ± 10
Little Molasses Cr., MI	43° 57.49'	84° 15.97'	12.5 ± 3.9	7.9 ± 0.13	90.4 ± 4.6	26.1 ± 0.4	137 ± 152	121 ± 4	114 ± 6

[1] Averages are calculated only until 8 October 2009 when the datasonde was buried in a flood

Table 2. Target chemistry for the five sediment used in the deployment. AVS and OC values are from a field survey and Ni amendment concentrations are target nominal concentrations. AVS = acid volatile sulfide, OC = organic carbon

			[Ni] amendment (mg kg^{-1} dw)		
Sediment type	AVS (µmol g^{-1})	OC (%)	Low	Med	High
Spring	0.8	0.4	57	172	517
Dow	1.3	1.1	210	630	1889
St. Joseph	14.1	0.6	456	913	1826
Raisin	0.4	2.8	518	1553	4658
Mill	46.1	2.4	1644	3287	6574

Table 3. Mean sediment chemistry (±1 SD) measured at deployment (day 0). AVS, OC, total Fe, and total Mn are means of the four Ni-amended sediment treatments. AVS = acid volatile sulfide, OC = organic carbon

			Total Fe	Total Mn	Total Ni (mg kg^{-1} dw)			
Sediment type	**AVS (µmol g^{-1})**	**OC (%)**	**(g kg^{-1} dw)**	**(g kg^{-1} dw)**	**Ref**	**Low**	**Med**	**High**
Spring	1.0 ± 0.9	0.47 ± 0.03	0.42 ± 0.06	0.15 ± 0.02	2.7	32	157	468
Dow	0.4 ± 0.1	1.1 ± 0.56	0.52 ± 0.11	0.10 ± 0.03	1.8	133	323	1382
St. Joseph	2.5 ± 1.2	1.3 ± 0.48	1.41 ± 0.59	0.29 ± 0.09	2.7	391	649	1170
Raisin	0.8 ± 0.8	0.69 ± 0.17	0.56 ± 0.12	0.23 ± 0.07	4.0	151	328	1143
Mill	29.8 ± 36.5	4.9 ± 1.3	21.64 ± 2.26	0.53 ± 0.01	18	1282	3105	4978

Table 4. P-values from *in situ* acute toxicity assays with *Hyalella azteca*. Each sediment type, habitat compartment, and endpoint was analyzed with a separate ANOVA comparing the four Ni treatments. For water column chambers, *H. azteca* were exposed to overlying water and sediment chambers were placed directly on the sediment surface. Significant and marginally significant p-values ($p < 0.10$) are bolded.

	Survival		Feeding	
Sediment	**Water column**	**Sediment**	**Water column**	**Sediment**
Spring (in Spring)	0.72	**0.08**	0.28	0.15
Spring (in L. Molasses)	0.75	0.88	0.49	0.33
Dow	0.90	**0.08**	0.69	0.63
St. Joseph	0.43	0.39	0.38	0.34
Raisin	0.27	0.78	0.23	**0.01**
Mill	0.79	0.27	0.33	0.48

Table 5. Summary of sediment physicochemical variables that best predicted Ni flux in deployed sediments measured with diffusive gradients in thin films (DGTs). Parameter selection was completed by stepwise multiple linear regression followed by model comparison with Akaike's Information Criterion. The ranking of variables (1° to 4°) indicates the order in which they were added to the model during stepwise selection. DGT flux was measured at three different time points and in three different vertical sections. AVS = acid volatile sulfide, SEM_{Mn} = simultaneously extracted Mn, OC = organic carbon, fOC = fraction (by weight) of organic carbon in sediment

Time	Section	1° variable	2° variable	3° variable	4° variable
Day 0	Water column	Total Ni			
	Surface	Total Ni			
	Deep	Porewater Ni	$CaCO_3$		
Week 4	Water column	Total Ni			
	Surface	Total Ni	AVS (deep)	SEM_{Mn} (deep)	Total Fe
	Deep	Total Ni	AVS (deep)	SEM_{Mn} (deep)	
Week 8	Water column	Density	OC (surface)		
	Surface	Total Ni	SEM_{Mn} (surface)		
	Deep	SEM_{Ni}-AVS/fOC (deep)			

Table 6. Summary of sediment physicochemical variables that best predicted indices of the colonizing benthic macroinvertebrate community. Parameter selection was completed by stepwise multiple linear regression followed by model comparison with Akaike's Information Criterion. The ranking of variables (1° to 3°) indicates the order in which they were added to the model during stepwise selection. Bolded values are those that include a measure of sediment Ni. The sign in brackets indicates whether the coefficient was positive or negative. EPT = Ephemeroptera, Plecoptera, and Trichoptera, SEM_{Ni} = simultaneously extracted Ni, AVS = acid volatile sulfide, SEM_{Mn} = simultaneously extracted Mn, K_d = Ni partitioning coefficient, fOC = fraction (by weight) of organic carbon in sediment, FeO_X+MnO_X = Fe and Mn oxides, OC = organic carbon

Time	Benthic index	1° variable	2° variable	3° variable
Week 4	Richness	**SEM_{Ni}/AVS (deep)** [-]	SEM_{Mn} (surface) [+]	**K_d** [-]
	Abundance	**SEM_{Ni} (deep)** [-]	**SEM_{Ni}/AVS (surface)** [+]	
	Diversity	**SEM_{Ni}-AVS/fOC (surface)** [-]	AVS (deep) [+]	
	EPT	**SEM_{Ni} (deep)** [-]	AVS (deep) [-]	
	Chironomids	FeO_X+MnO_X (surface) [-]		
	Gammarus	**SEM_{Ni} (deep)** [-]	SEM_{Mn} (surface) [-]	
Week 8	Richness	Total Fe [-]	Density [+]	AVS (surface) [+]
	Abundance	**SEM_{Ni} (surface)** [-]	Total Fe [-]	
	Diversity	Density [+]	SEM_{Mn} (deep) [+]	
	EPT	TOC (surface) [-]	AVS (deep) [+]	
	Chironomids	SEM_{Mn} (deep) [-]	Density [-]	**SEM_{Ni} (surface)** [-]
	Gammarus	*none*		

Table 7. Pearson's R coefficients for correlations between Ni flux as measured by diffusive gradients in thin films (DGTs) and benthic indices. No correlations are significant; a value > 0.44 or < -0.44 indicates a significant correlation (df = 18, $\alpha = 0.05$). EPT = Ephemeroptera, Plecoptera, and Trichoptera

DGT measurement	Richness	Abundance	Diversity	EPT abundance	Chironomids	Gammarus
Ni flux (water column)	-0.09	0.01	-0.01	-0.03	-0.23	0.01
Ni flux (surface)	-0.29	-0.12	-0.19	-0.05	-0.20	-0.23
Ni flux (deep)	-0.36	-0.12	-0.29	-0.12	-0.14	-0.28

Figures

Figure 1. Colonization baskets within mesh bags (A) and chambers used for *in situ* toxicity testing (B).

Figure 2. Ni flux as measured with diffusive gradients in thin films (DGTs). Each panel represents a different sampling date and groups of bars are different sediment types with increasing Ni treatments from left to right. Shading within the stacked bars represents flux in the different vertical sections of the DGT. Note the change in scale on y-axis in each panel.

Figure 3. Mn flux as measured with diffusive gradients in thin films (DGTs). Each panel represents a different sampling date and groups of bars are different sediment types with increasing Ni treatments from left to right. Shading within the stacked bars represents flux in the different vertical sections of the DGT.

Figure 4. Fe flux as measured with diffusive gradients in thin films (DGTs). Each panel represents a different sampling date and groups of bars are different sediment types with increasing Ni treatments from left to right. Shading within the stacked bars represents flux in the different vertical sections of the DGT.

Figure 5. Relationship between Ni partitioning coefficient (K_d) and significant sediment physicochemical variables as predicted by stepwise multiple linear regression during three sampling times. For day 0 and week 8 plots (A and C, respectively), the x-axis are predicted K_d values from the best-fit models. The solid line in A and C is a 1:1 line and predicted values that fall on this line are the same as observed. At week 4 (B), total Fe, which was the only sediment physicochemical variable that predicted K_d, is on the x-axis and the solid line represents the best-fit line from least-squares regression. OC = organic carbon, SEM_{Mn} = simultaneously extracted Mn, FeO_X+MnO_X = Fe and Mn oxides

Figure 6. Relationship between log SEM_{Ni}/AVS of deep sediment and taxa richness of the colonizing macroinvertebrate communitiy at week 4. The solid line represents the best-fit line determined from least-squares regression. Each sediment type is represented by a different symbol and Ni treatment categories are represented by colors. SEM-AVS theory predicts that for sediments with a SEM_{Ni}/AVS ratio below 1 (dotted vertical line) there should be no free metal and thus no toxicity. SEM_{Ni} = simulataneously extracted Ni, AVS = acid volatile sulfide

Figure 7. Relationship between SEM_{Ni}-AVS/fOC of surface sediment and Shannon diversity of the colonizing macroinvertebrate community at week 4. SEM_{Ni}-AVS/fOC values were log + 1 transformed after negative values were converted to 0. Each sediment type is represented by a different symbol and Ni treatment categories are represented by colors. SEM-AVS theory predicts that for sediments with SEM_{Ni}-AVS/fOC below 100-150 µmol g^{-1} (shaded box) should be nontoxic. SEM_{Ni} = simulataneously extracted Ni, AVS = acid volatile sulfide, fOC = fraction (by weight) of organic carbon in sediment

Figure 8. Relationship between log SEM_{Ni} of deep sediment and Gammarus abundance (as a percent of reference sediments) at week 4. The solid line represents the best-fit line from binomial logistic regression and the dotted line is the 95% confidence interval of the line. Each sediment type is represented by a different symbol and Ni treatment categories are represented by colors. SEM_{Ni} = simultaneously extracted Ni

Figure 1

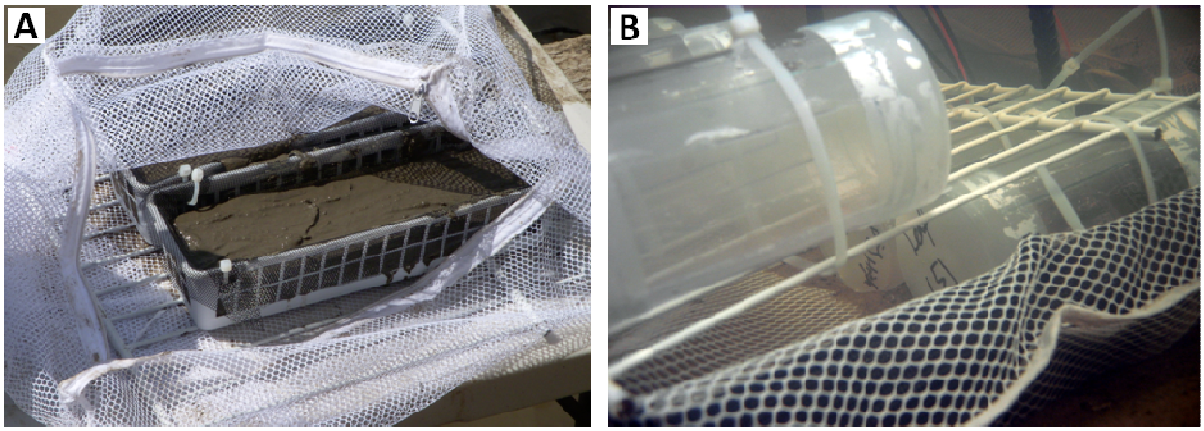

Figure 2

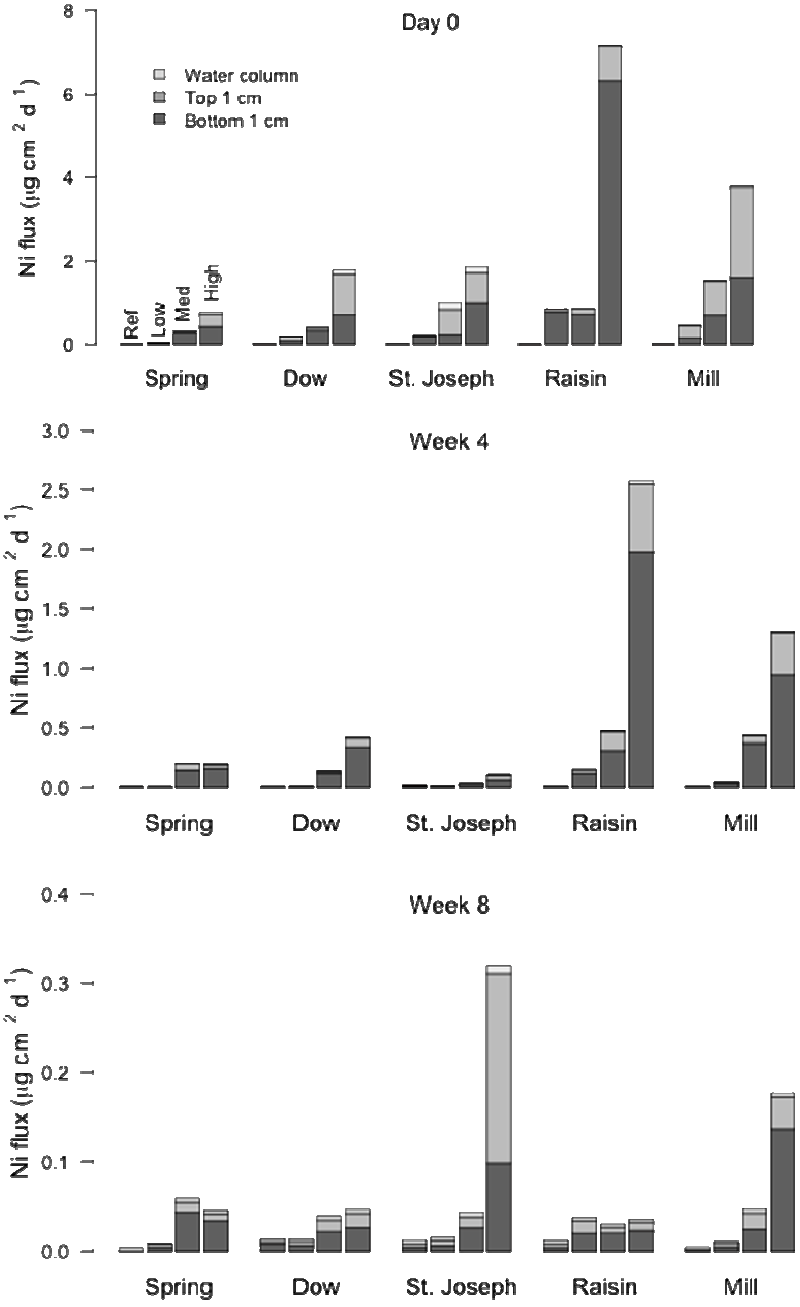
Day 0
Water column
Top 1 cm
Bottom 1 cm
Ni flux (µg cm $^{-2}$ d $^{-1}$)
Ref
Low
Med
High
Spring
Dow
St. Joseph
Raisin
Mill
Week 4
Week 8

Figure 3

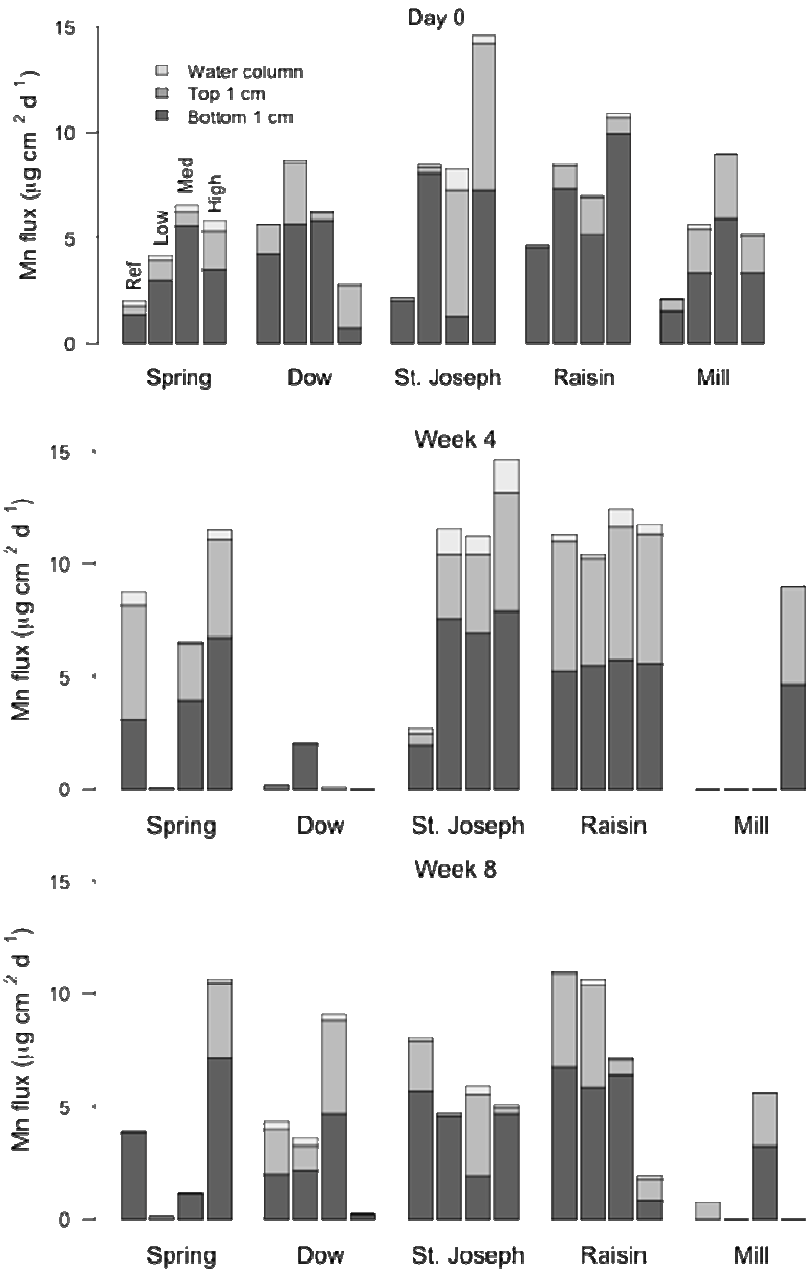
Day 0
Water column
Top 1 cm
Bottom 1 cm
Ref
Low
Med
High
Mn flux (µg cm $^{-2}$ d $^{-1}$)
15
10
5
0
Spring
Dow
St. Joseph
Raisin
Mill
Week 4
Week 8

Figure 4

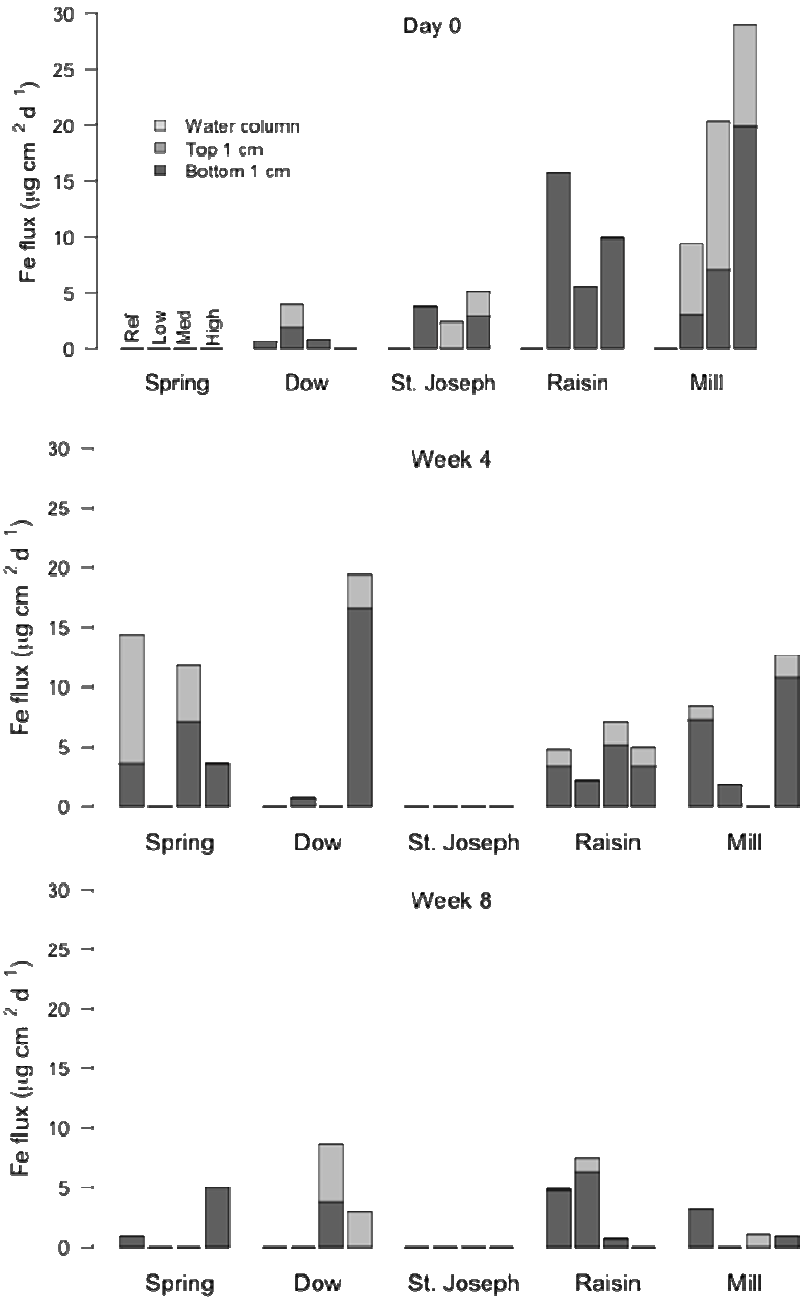
Day 0
Water column
Top 1 cm
Bottom 1 cm
Fe flux (µg cm $^{-2}$ d $^{-1}$)
Ref
Low
Med
High
Spring
Dow
St. Joseph
Raisin
Mill
Week 4
Week 8

Figure 5

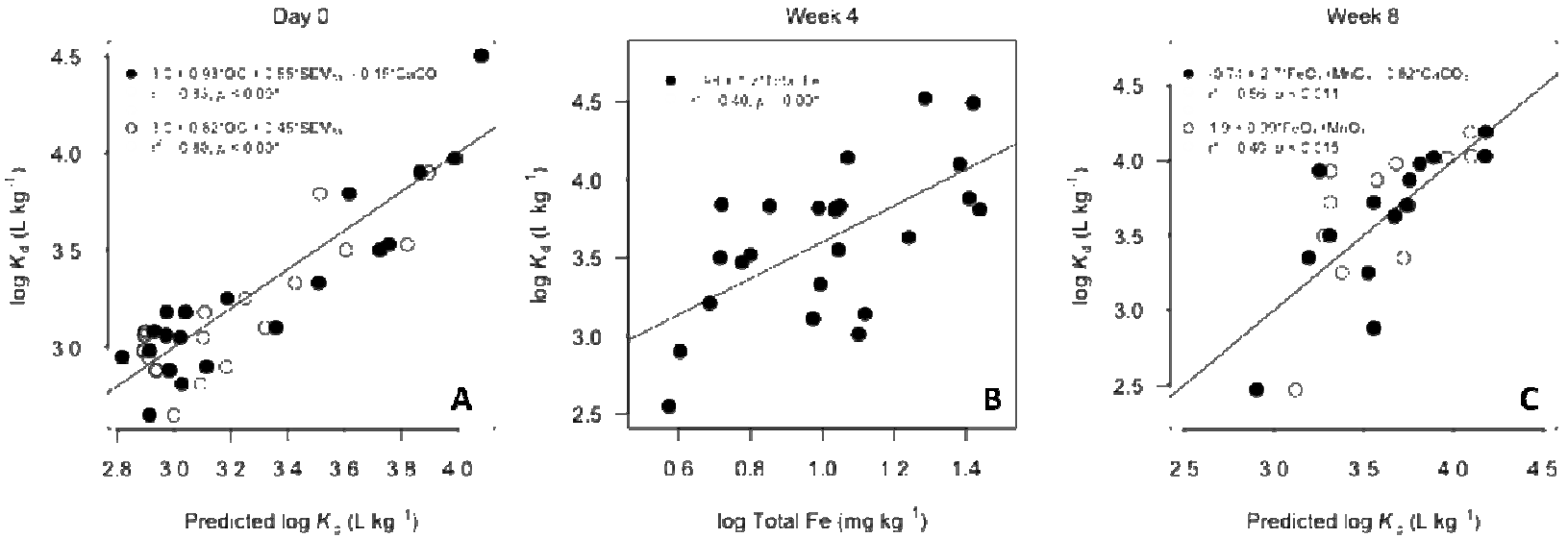
Day 0
Week 4
Week 8
log K_d (L kg^{-1})
Predicted log K_d (L kg^{-1})
log Total Fe (mg kg^{-1})
A
B
C

Figure 6

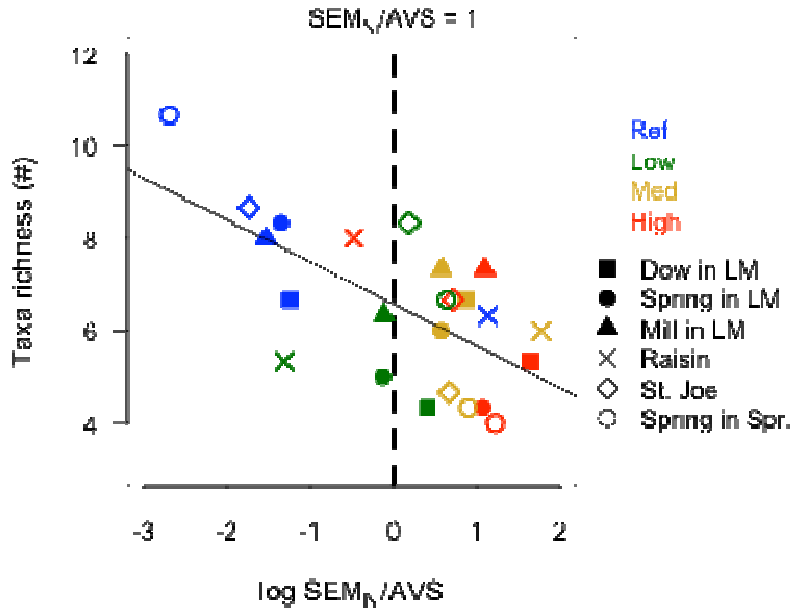

Figure 7

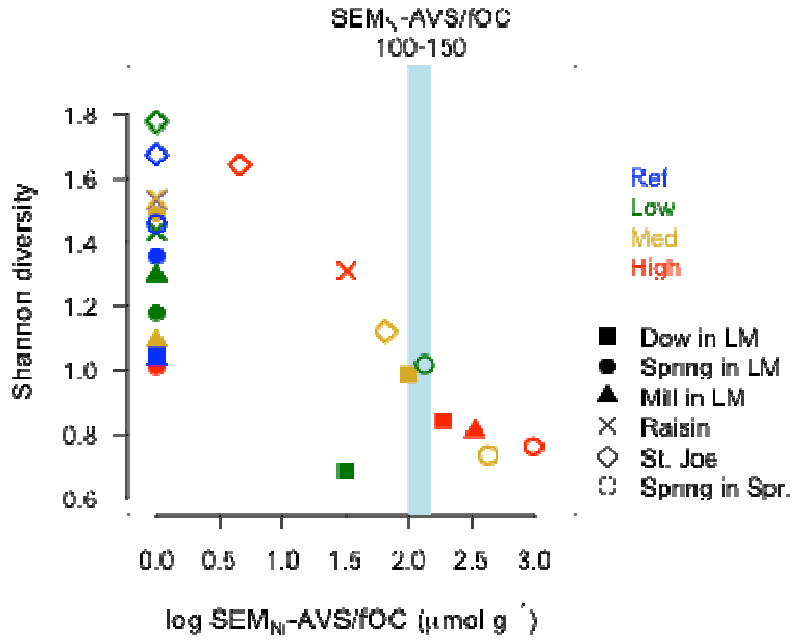

Figure 8

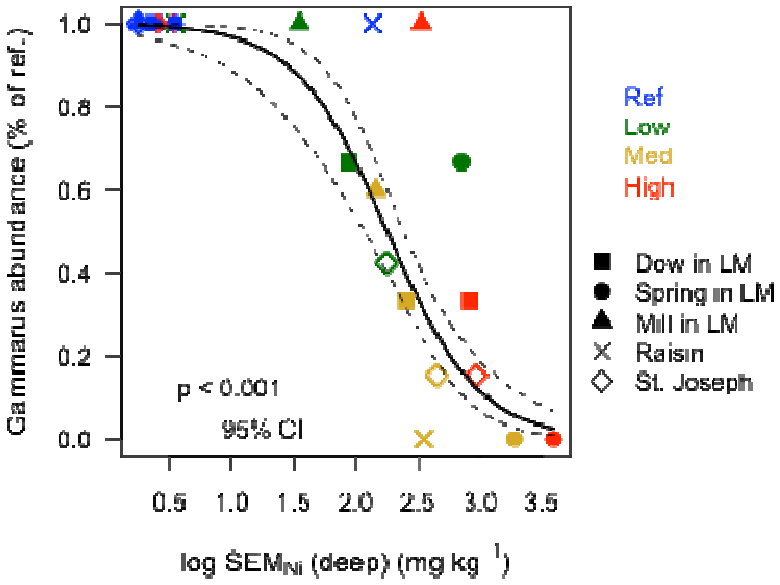
Gammarus abundance (% of ref.)
1.0
0.8
0.6
0.4
0.2
0.0
p < 0.001
95% CI
0.5
1.0
1.5
2.0
2.5
3.0
3.5
log SEM$_{Ni}$ (deep) (mg kg^{-1})
Ref
Low
Med
High
Dow in LM
Spring in LM
Mill in LM
Raisin
St. Joseph

Appendices

Table A1. Statistics for the suite of models used in model selection for Ni flux measured at deployment (day 0). Ni flux was measured in three vertical sections with diffusing gradient in thin films (DGTs). Akaike's Information Criterion (AIC) was used to select the best model and models with sample size corrected AIC values (AICc) < 2 from the lowest AICc are considered potential "best" models. AIC weights (ω_i) indicate the probability that a particular model is the best model of the entire suite. Models in bold red text were produced from a stepwise multiple linear regression, which included all the sediment physicochemical parameters measured.

log DGT flux (water column) - day 0

Explanatory variable(s)	**p**	**r^2**	**AICc**	**ω_i**
Total Ni	< 0.001	0.53	62.6	0.32
Porewater Ni	< 0.001	0.53	62.7	0.30
SEM_{Ni} (deep)	< 0.001	0.51	63.7	0.19
SEM_{Ni}-AVS (deep)	0.001	0.50	64.0	0.16
SEM_{Ni}-AVS/fOC (deep)	0.005	0.37	68.6	0.02
SEM_{Ni}/AVS (deep)	0.010	0.32	70.1	0.01
K_d	0.177	0.10	75.7	0.00
Stream	0.285	0.09	79.0	0.00

log DGT flux (surface) - day 0

Explanatory variable(s)	**p**	**r^2**	**AICc**	**ω_i**
Total Ni	< 0.001	0.86	57.3	0.86
Porewater Ni	< 0.001	0.82	62.1	0.08
SEM_{Ni} (deep)	< 0.001	0.82	62.3	0.07
SEM_{Ni}-AVS (deep)	< 0.001	0.55	80.1	0.00
SEM_{Ni}/AVS (deep)	< 0.001	0.54	80.9	0.00
SEM_{Ni}-AVS/fOC (deep)	0.001	0.49	82.9	0.00
K_d	0.056	0.19	92.1	0.00
Stream	0.95	0.00	99.4	0.00

log DGT flux (deep) - day 0

Explanatory variable(s)	**p**	**r^2**	**AICc**	**ω_i**
Porewater Ni	< 0.001	0.87	56.8	0.48
Porewater Ni + $CaCO_3$	< 0.001	0.89	57.1	0.41
SEM_{Ni} (deep)	< 0.001	0.85	59.9	0.10
Total Ni	< 0.001	0.82	63.2	0.02
SEM_{Ni}/AVS (deep)	< 0.001	0.65	77.3	0.00
SEM_{Ni}-AVS/fOC (deep)	< 0.001	0.63	78.0	0.00
SEM_{Ni}-AVS (deep)	< 0.001	0.52	83.5	0.00
K_d	0.149	0.11	95.6	0.00
Stream	0.834	0.05	100.1	0.00

Table A2. Statistics for the suite of models used in model selection for colonizing benthic macroinvertebrate indices and Ni flux measured at week 4. Akaike's Information Criterion (AIC) was used to select the best model and models with sample size corrected AIC values (AICc) < 2 from the lowest AICc are considered potential "best" models. AIC weights (ω_i) indicate the probability that a particular model is the best model of the entire suite. For some benthic indices, the stream where baskets were deployed was significant and was included as a blocking factor (noted at top of table). Models in bold red text were produced from a stepwise multiple linear regression, which included all the sediment physicochemical parameters measured. Ni flux was measured in three vertical sections with diffusing gradient in thin films (DGTs).

Total taxa – Week 4

Explanatory variable(s)	**p**	**r^2**	**AICc**	**ω_i**
SEM_{Ni}/AVS (deep)	0.001	0.42	85.8	0.35
SEM_{Ni}/AVS (deep) + SEM_{Mn} (top)	0.001	0.47	86.7	0.23
SEM_{Ni}/AVS (deep) + SEM_{Mn} (top) + K_d	0.002	0.52	87.6	0.14
SEM_{Ni} (deep)	0.002	0.36	88.0	0.12
Total Ni	0.005	0.30	90.2	0.04
SEM_{Ni}-AVS (deep)	0.005	0.30	90.2	0.04
K_d	0.010	0.27	91.4	0.02
SEM_{Ni}-AVS/fOC (deep)	0.015	0.24	92.3	0.01
Porewater Ni	0.027	0.20	93.4	0.01
SEM_{Ni} (surface)	0.028	0.20	93.4	0.01
SEM_{Ni}/AVS (surface)	0.034	0.19	93.7	0.01
SEM_{Ni}-AVS (surface)	0.031	0.19	93.8	0.01
SEM_{Ni}-AVS/fOC (surface)	0.054	0.16	94.7	0.00
Stream	0.588	0.04	103.9	0.00

Abundance (+ STREAM BLOCK) – Week 4

Explanatory variable(s)	**p**	**r^2**	**AICc**	**ω_i**
SEM_{Ni} (deep) +SEM_{Ni}/AVS (surface)	0.005	0.57	221.0	0.36
SEM_{Ni} (deep)	0.007	0.50	221.0	0.35
SEM_{Ni}-AVS (deep)	0.029	0.42	224.3	0.07
Porewater Ni	0.033	0.41	224.6	0.06
Total Ni	0.034	0.41	224.7	0.06
SEM_{Ni}/AVS (deep)	0.045	0.40	225.3	0.04
Stream	0.117	0.25	226.9	0.02
SEM_{Ni}-AVS/fOC (deep)	0.097	0.35	226.9	0.02
K_d	0.144	0.33	227.7	0.01
SEM_{Ni}-AVS (surface)	0.205	0.31	228.4	0.01
SEM_{Ni} (surface)	0.280	0.30	229.0	0.01
SEM_{Ni}/AVS (surface)	0.531	0.27	230.0	0.00
SEM_{Ni}-AVS/fOC (surface)	0.597	0.26	230.1	0.00

Table A2 (cont.)

Shannon diversity (+ STREAM) – Week 4

Explanatory variable(s)	p	r^2	AICc	ω_i
SEM_{Ni}-AVS/fOC (surface)	< 0.001	0.80	-9.1	0.49
SEM_{Ni}-AVS/fOC (surface) + AVS (deep)	< 0.001	0.83	-8.4	0.34
SEM_{Ni}/AVS (surface)	0.001	0.78	-6.4	0.12
SEM_{Ni} (surface)	0.002	0.74	-3.3	0.03
SEM_{Ni}-AVS (surface)	0.003	0.73	-2.4	0.02
Total Ni	0.014	0.69	1.4	0.00
K_d	0.022	0.68	2.3	0.00
SEM_{Ni}-AVS (deep)	0.022	0.68	2.4	0.00
SEM_{Ni}/AVS (deep)	0.028	0.67	2.9	0.00
Porewater Ni	0.048	0.65	4.1	0.00
SEM_{Ni} (deep)	0.057	0.65	4.4	0.00
SEM_{Ni}-AVS/fOC (deep)	0.070	0.64	4.9	0.00
Stream	0.001	0.57	5.5	0.00

EPT abundance – Week 4

Explanatory variable(s)	p	r^2	AICc	ω_i
SEM_{Ni} (deep) + AVS (deep)	0.011	0.35	137.4	0.46
SEM_{Ni} (deep)	0.016	0.24	140.3	0.11
SEM_{Ni} (deep) + AVS (deep) + SEM_{Fe} (surface)	0.015	0.40	140.6	0.10
SEM_{Ni} (deep) + AVS (deep) + SEM_{Fe} (surface) + AVS (surface)	0.012	0.48	140.9	0.08
K_d	0.028	0.20	141.4	0.06
Total Ni	0.052	0.16	142.6	0.04
SEM_{Ni}-AVS (deep)	0.053	0.16	142.6	0.03
SEM_{Ni} (deep) + AVS (deep) + SEM_{Fe} (surface) + AVS (surface) + K_d	0.013	0.53	142.7	0.03
SEM_{Ni}-AVS/fOC (deep)	0.098	0.12	143.8	0.02
SEM_{Ni}/AVS (deep)	0.171	0.08	144.7	0.01
SEM_{Ni} (surface)	0.177	0.08	144.8	0.01
SEM_{Ni}-AVS (surface)	0.178	0.08	144.8	0.01
Porewater Ni	0.194	0.08	144.8	0.01
SEM_{Ni}-AVS/fOC (surface)	0.241	0.06	145.3	0.01
SEM_{Ni}/AVS (surface)	0.547	0.02	146.4	0.01
Stream	0.150	0.47	149.0	0.00

Table A2 (cont.)

Chironomidae (+ STREAM) – Week 4

Explanatory variable(s)	p	r^2	AICc	ω_i
FeO_X+MnO_X (surface)	0.013	0.69	200.8	0.60
Stream	0.001	0.57	205.2	0.07
SEM_{Ni} (deep)	0.110	0.62	205.52	0.06
Porewater Ni	0.112	0.62	205.6	0.06
Total Ni	0.116	0.62	205.6	0.05
SEM_{Ni}-AVS (deep)	0.179	0.61	206.5	0.04
SEM_{Ni}-AVS (surface)	0.244	0.60	207.1	0.03
K_d	0.278	0.59	207.3	0.02
SEM_{Ni}/AVS (deep)	0.299	0.59	207.4	0.02
SEM_{Ni} (surface)	0.329	0.59	207.6	0.02
SEM_{Ni}-AVS/fOC (deep)	0.554	0.57	208.4	0.01
SEM_{Ni}/AVS (surface)	0.728	0.57	208.7	0.01
SEM_{Ni}-AVS/fOC (surface)	0.752	0.57	208.7	0.01

Gammarus (+ STREAM) – Week 4

Explanatory variable(s)	p	r^2	AICc	ω_i
SEM_{Ni} (deep)	0.009	0.65	121.0	0.33
SEM_{Ni} (deep) + SEM_{Mn} (surface)	0.001	0.68	122.8	0.13
SEM_{Ni}-AVS/fOC (deep)	0.024	0.62	123.2	0.11
Total Ni	0.026	0.61	123.4	0.10
SEM_{Ni}-AVS (deep)	0.030	0.61	123.6	0.09
SEM_{Ni}/AVS (deep)	0.030	0.61	123.7	0.09
K_d	0.049	0.59	124.8	0.05
Porewater Ni	0.061	0.58	125.2	0.04
Stream	0.003	0.50	126.2	0.02
SEM_{Ni} (surface)	0.118	0.56	126.6	0.02
SEM_{Ni}/AVS (surface)	0.200	0.54	127.6	0.01
SEM_{Ni}-AVS/fOC (surface)	0.224	0.53	127.8	0.01
SEM_{Ni}-AVS (surface)	0.325	0.52	128.5	0.01

Table A2 (cont.)

log DGT flux (water column) – Week 4

Explanatory variable(s)	p	r^2	AICc	ω_i
Total Ni	0.003	0.39	33.3	0.39
K_d	0.004	0.37	33.6	0.33
SEM_{Ni} (surface)	0.017	0.28	36.5	0.08
Porewater Ni	0.036	0.22	38.0	0.04
SEM_{Ni}/AVS (surface)	0.050	0.20	38.6	0.03
SEM_{Ni}-AVS/fOC (surface)	0.050	0.20	38.6	0.03
SEM_{Ni}-AVS (surface)	0.095	0.15	39.8	0.01
SEM_{Ni}-AVS (deep)	0.119	0.13	40.2	0.01
SEM_{Ni}/AVS (deep)	0.211	0.09	41.2	0.01
SEM_{Ni} (deep)	0.367	0.05	42.1	0.00
SEM_{Ni}-AVS/fOC (deep)	0.368	0.05	42.1	0.00
Stream	0.595	0.11	43.8	0.00

log DGT flux (surface) – Week 4

Explanatory variable(s)	p	r^2	AICc	ω_i
Total Ni + AVS (deep) + SEM_{Mn} (deep) + Total Fe	< 0.001	0.75	66.4	0.39
Total Ni	< 0.001	0.53	67.4	0.24
Total Ni + AVS (deep) + SEM_{Mn} (deep)	< 0.001	0.67	68.0	0.17
Total Ni + AVS (deep)	0.001	0.59	68.5	0.14
Porewater Ni	0.001	0.44	71.4	0.03
SEM_{Ni} (surface)	0.005	0.36	74.1	0.01
K_d	0.009	0.32	75.3	0.00
SEM_{Ni}-AVS (deep)	0.017	0.28	76.5	0.00
SEM_{Ni}-AVS (surface)	0.020	0.26	76.9	0.00
SEM_{Ni}/AVS (surface)	0.022	0.26	77.0	0.00
SEM_{Ni}-AVS/fOC (surface)	0.034	0.23	77.9	0.00
SEM_{Ni}/AVS (deep)	0.048	0.20	78.6	0.00
SEM_{Ni} (deep)	0.110	0.14	80.1	0.00
SEM_{Ni}-AVS/fOC (deep)	0.117	0.13	80.2	0.00
Stream	0.310	0.13	83.5	0.00

Table A2 (cont.)

log DGT flux (deep) – Week 4

Explanatory variable(s)	p	r^2	AICc	ω_i
Total Ni	< 0.001	0.66	73.7	0.33
Total Ni + AVS (deep)	< 0.001	0.70	74.0	0.29
Total Ni + AVS (deep) + SEM_{Mn} (deep)	< 0.001	0.73	75.5	0.14
Total Ni + AVS (deep) + SEM_{Mn} (deep) + Total Fe	< 0.001	0.77	76.1	0.10
Total Ni + AVS (deep) + SEM_{Mn} (deep) + Total Fe + FeO_X+MnO_X (surface)	< 0.001	0.81	77.6	0.05
Porewater Ni	< 0.001	0.60	76.4	0.09
SEM_{Ni} (surface)	0.002	0.43	83.6	0.00
SEM_{Ni}-AVS/fOC (surface)	0.005	0.37	85.8	0.00
SEM_{Ni}/AVS (surface)	0.006	0.35	86.4	0.00
SEM_{Ni}-AVS (surface)	0.006	0.35	86.5	0.00
SEM_{Ni}-AVS (deep)	0.006	0.35	86.5	0.00
K_d	0.007	0.34	86.7	0.00
SEM_{Ni}/AVS (deep)	0.022	0.26	89.0	0.00
SEM_{Ni}-AVS/fOC (deep)	0.042	0.21	90.3	0.00
SEM_{Ni} (deep)	0.044	0.21	90.4	0.00
Stream	0.419	0.10	96.1	0.00

Table A3. Statistics for the suite of models used in model selection for colonizing benthic macroinvertebrate indices and Ni flux measured at week 8. Akaike's Information Criterion (AIC) was used to select the best model and models with sample size corrected AIC values (AICc) < 2 from the lowest AICc are considered potential "best" models. AIC weights (ω_i) indicate the probability that a particular model is the best model of the entire suite. For some benthic indices, the stream where baskets were deployed was significant and was included as a blocking factor (noted at top of table). Models in bold red text were produced from a stepwise multiple linear regression, which included all the sediment physicochemical parameters measured. Ni flux was measured in three vertical sections with diffusing gradient in thin films (DGTs).

Total taxa (+ STREAM BLOCK) – Week 8

Explanatory variable(s)	**p**	**r^2**	**AICc**	**ω_i**
Total Fe + Density + AVS (surface)	< 0.005	0.87	63.5	0.62
Total Fe + Density + AVS (surface) + Total Mn	< 0.006	0.89	65.9	0.19
Total Fe + SEM_{Ni}-AVS (surface)	< 0.002	0.79	67.8	0.07
Total Fe + SEM_{Ni}-AVS (surface) + Density + AVS (surface)	< 0.004	0.87	69.1	0.04
Total Fe + SEM_{Ni}-AVS (surface) + Density	< 0.003	0.82	70.2	0.02
Total Fe + Density + AVS (surface) + Total Mn + SEM_{Ni}/AVS (surface)	< 0.007	0.91	70.3	0.02
Total Fe	< 0.001	0.71	70.6	0.02
SEM_{Ni}-AVS (surface)	< 0.001	0.69	71.5	0.01
SEM_{Ni} (surface)	< 0.001	0.68	72.2	0.01
SEM_{Ni}/AVS (surface)	< 0.001	0.66	73.9	0.00
Total Ni	0.002	0.60	76.8	0.00
SEM_{Ni}-AVS/fOC (surface)	0.002	0.60	76.9	0.00
SEM_{Ni}-AVS (deep)	0.002	0.58	77.8	0.00
SEM_{Ni} (deep)	0.003	0.57	78.3	0.00
Stream	0.004	0.48	78.5	0.00
SEM_{Ni}-AVS/fOC (deep)	0.004	0.55	79.1	0.00
SEM_{Ni}/AVS (deep)	0.006	0.53	80.2	0.00

Abundance (+ STREAM BLOCK) – Week 8

Explanatory variable(s)	**p**	**r^2**	**AICc**	**ω_i**
SEM_{Ni} (surface)	< 0.001	0.69	181.1	0.31
SEM_{Ni} (surface) + Total Fe	< 0.001	0.75	181.4	0.28
SEM_{Ni}/AVS (surface)	< 0.001	0.67	182.6	0.15
SEM_{Ni}-AVS/fOC (surface)	0.001	0.63	184.5	0.06
SEM_{Ni}-AVS (surface)	0.001	0.63	184.8	0.05
Total Ni	0.001	0.62	185.0	0.05
Stream	0.001	0.54	185.4	0.04
SEM_{Ni}-AVS/fOC (deep)	0.002	0.60	186.3	0.02
SEM_{Ni} (deep)	0.002	0.60	186.3	0.02
SEM_{Ni}-AVS (deep)	0.002	0.59	186.9	0.02
SEM_{Ni}/AVS (deep)	0.003	0.57	187.5	0.01

Table A3 (cont.)

Shannon diversity (+ STREAM) – Week 8

Explanatory variable(s)	p	r^2	AICc	ω_i
Density + SEM_{Mn} (deep)	< 0.001	0.84	-5.7	0.56
Density + SEM_{Mn} (deep) + SEM_{Mn} (surface)	< 0.001	0.86	-3.7	0.20
Density	< 0.001	0.76	-1.7	0.08
Density + SEM_{Mn} (deep) + SEM_{Mn} (surface) + SEM_{Ni}/AVS (surface)	< 0.001	0.88	-1.3	0.06
SEMNi (deep)	< 0.001	0.72	1.26	0.02
Total Ni	< 0.001	0.72	1.3	0.02
SEMNi-AVS/fOC (deep)	< 0.001	0.71	1.8	0.01
SEMNi/AVS (deep)	< 0.001	0.70	2.2	0.01
SEMNi (surface)	< 0.001	0.70	2.3	0.01
SEMNi-AVS (deep)	< 0.001	0.70	2.6	0.01
Stream	< 0.001	0.63	2.7	0.01
SEMNi-AVS (surface)	< 0.001	0.68	3.6	0.01
SEMNi/AVS (surface)	< 0.001	0.68	3.7	0.01
SEMNi-AVS/fOC (surface)	0.001	0.65	5.4	0.00

EPT abundance (+ STREAM) – Week 8

Explanatory variable(s)	p	r^2	AICc	ω_i
OC (surface) + AVS (deep)	< 0.001	0.88	115.8	0.61
OC (surface)	< 0.001	0.84	116.8	0.38
Stream	< 0.001	0.71	125.4	0.01
SEM_{Ni}-AVS (surface)	< 0.001	0.72	128.0	0.00
SEM_{Ni}-AVS (deep)	< 0.001	0.72	128.2	0.00
SEM_{Ni} (surface)	< 0.001	0.72	128.3	0.00
Total Ni	< 0.001	0.71	128.8	0.00
SEM_{Ni}/AVS (deep)	< 0.001	0.71	128.9	0.00
SEM_{Ni} (deep)	< 0.001	0.71	128.9	0.00
SEM_{Ni}-AVS/fOC(surface)	< 0.001	0.71	129.0	0.00
SEM_{Ni}/AVS (surface)	< 0.001	0.71	129.0	0.00
SEM_{Ni}-AVS/fOC(deep)	< 0.001	0.71	129.0	0.00

Table A3 (cont.)

Chironomidae (+ STREAM) – Week 8

Explanatory variable(s)	p	r^2	AICc	ω_i
SEM_{Mn} (deep) + Density + SEM_{Ni} (surface)	< 0.001	0.93	157.4	0.79
SEM_{Mn} (deep) + Density	< 0.001	0.88	162.2	0.07
Stream	< 0.001	0.80	164.0	0.03
SEM_{Mn} (deep)	< 0.001	0.84	164.1	0.03
SEM_{Ni} (surface)	< 0.001	0.83	165.1	0.02
SEM_{Ni}-AVS/fOC (surface)	< 0.001	0.82	165.4	0.01
SEM_{Ni}/AVS (surface)	< 0.001	0.82	165.7	0.01
Total Ni	< 0.001	0.82	166.2	0.01
SEM_{Ni}-AVS (surface)	< 0.001	0.82	166.3	0.01
SEM_{Ni} (deep)	< 0.001	0.81	166.6	0.01
SEM_{Ni}-AVS/fOC (deep)	< 0.001	0.81	166.7	0.01
SEM_{Ni}-AVS (deep)	< 0.001	0.81	167.0	0.01
SEM_{Ni}/AVS (deep)	< 0.001	0.81	167.4	0.01

Gammarus (+ STREAM) – Week 8

Explanatory variable(s)	p	r^2	AICc	ω_i
Stream	< 0.001	0.95	78.5	0.26
SEM_{Ni}-AVS/fOC (deep)	< 0.001	0.96	79.4	0.17
SEM_{Ni} (deep)	< 0.001	0.96	80.0	0.12
SEM_{Ni}/AVS (deep)	< 0.001	0.96	80.2	0.11
Total Ni	< 0.001	0.96	80.2	0.11
SEM_{Ni}-AVS (deep)	< 0.001	0.95	81.5	0.06
SEM_{Ni}-AVS (surface)	< 0.001	0.95	81.9	0.05
SEM_{Ni} (surface)	< 0.001	0.95	82.0	0.04
SEM_{Ni}/AVS (surface)	< 0.001	0.95	82.1	0.04
SEM_{Ni}-AVS/fOC (surface)	< 0.001	0.95	82.1	0.04

log DGT flux (water column) (+ STREAM) – Week 8

Explanatory variable(s)	p	r^2	AICc	ω_i
Density + OC (surface)	0.009	0.57	20.0	0.36
Density + OC (surface) + Total Fe	0.009	0.63	22.1	0.13
Density	0.036	0.40	22.6	0.10
Stream	0.066	0.27	22.9	0.08
SEM_{Ni}-AVS/fOC (deep)	0.043	0.39	23.0	0.08
SEM_{Ni}-AVS (deep)	0.052	0.38	23.5	0.06
SEM_{Ni}-AVS/fOC (surface)	0.070	0.35	24.4	0.04
SEM_{Ni} (deep)	0.082	0.33	24.8	0.03
Total Ni	0.083	0.33	24.9	0.03
SEM_{Ni}-AVS (surface)	0.085	0.33	24.9	0.03
SEM_{Ni}/AVS (deep)	0.112	0.31	25.7	0.02
SEM_{Ni} (surface)	0.134	0.29	26.2	0.02
SEM_{Ni}/AVS (surface)	0.151	0.29	26.2	0.02

Table A3 (cont.)

log DGT flux (surface) – Week 8

Explanatory variable(s)	**p**	**r^2**	**AICc**	**ω_i**
Total Ni	< 0.001	0.54	56.7	0.30
SEM_{Ni} (surface)	< 0.001	0.54	57.1	0.25
Total Ni + SEM_{Mn} (surface)	< 0.001	0.60	57.5	0.20
SEM_{Ni} (deep)	0.001	0.49	59.0	0.09
SEM_{Ni}-AVS/fOC (deep)	0.001	0.46	59.9	0.06
SEM_{Ni}/AVS (surface)	0.002	0.44	60.7	0.04
SEM_{Ni}/AVS (deep)	0.003	0.41	61.6	0.03
SEM_{Ni}-AVS (deep)	0.003	0.40	61.8	0.02
SEM_{Ni}-AVS/fOC (surface)	0.008	0.35	63.6	0.01
SEM_{Ni}-AVS (surface)	0.013	0.31	64.6	0.01
Stream	0.867	0.02	74.5	0.00

log DGT flux (deep) – Week 8

Explanatory variable(s)	**p**	**r^2**	**AICc**	**ω_i**
SEM_{Ni}-AVS/fOC (deep)	< 0.001	0.57	65.6	0.29
SEM_{Ni}/AVS (deep)	< 0.001	0.57	65.8	0.27
SEM_{Ni} (deep)	< 0.001	0.56	66.1	0.23
Total Ni	< 0.001	0.55	66.7	0.17
SEM_{Ni}-AVS (deep)	0.001	0.46	70.2	0.03
SEM_{Ni} (surface)	0.007	0.34	74.3	0.00
SEM_{Ni}-AVS/fOC (surface)	0.008	0.33	74.6	0.00
SEM_{Ni}/AVS (surface)	0.012	0.31	75.2	0.00
SEM_{Ni}-AVS (surface)	0.026	0.25	76.9	0.00
Stream	0.79	0.03	85.1	0.00

Table A4. Statistics and parameters for the best model(s) predicting Ni partitioning coefficient (K_d) in deployed sediments during three sampling times. Akaike's Information Criterion (AIC) was used to select the best model and models with sample size corrected AIC values (AICc) < 2 from the lowest AICc are considered potential "best" models. AIC weights (ω_i) indicate the probability that a particular model is the best model of the entire suite. Parameters were selected using stepwise multiple linear regression.

Day 0

Parameter	Coefficient	SE	p-value	r^2	AIC_c	ω_i
Model 1				0.83	-1.89	0.44
OC (deep)	0.93	0.15	< 0.001			
SEM_{Mn} (deep)	0.55	0.2	0.013			
$CaCO_3$	-0.15	0.08	0.10			
$\log(K_d) = 3.0 + 0.93*\log(OC) + 0.55*\log(SEM_{Mn}) - 0.15*\log(CaCO_3)$						
Model 2				0.80	-1.78	0.42
OC (deep)	0.82	0.14	< 0.001			
SEM_{Mn} (deep)	0.45	0.20	0.039			
$\log(K_d) = 3.0 + 0.82*\log(OC) + 0.45*\log(SEM_{Mn})$						

Week 4

Parameter	Coefficient	SE	p-value	r^2	AIC_c	ω_i
Model 1				0.40	26.5	0.42
Total Fe	1.2	0.30	0.001			
$\log(K_d) = 0.98 + 1.2*\log(\text{Tot Fe})$						
Model 2				0.46	27.1	0.31
Total Fe	1.3	0.32	0.001			
AVS (deep)	-0.23	0.16	0.16			
$\log(K_d) = 0.56 + 1.3*\log(\text{Tot Fe}) - 0.23*\log(AVS)$						
Model 3				0.52	27.4	0.27
Total Fe	1.2	0.32	0.001			
AVS (deep)	-0.25	0.15	0.12			
OC (surface)	0.58	0.36	0.12			
$\log(K_d) = 0.57 + 1.2*\log(\text{Tot Fe}) - 0.25*\log(AVS) + 0.58*\log(OC)$						

Table A4 (cont.)

Week 8

Parameter	Coefficient	SE	p-value	r^2	AIC_c	ω_i
Model 1				0.56	19.4	0.42
FeO_X+MnO_X (deep)	2.7	0.90	0.013			
$CaCO_3$	-0.82	0.41	0.073			
$\log(K_d) = -0.74 + 2.7*\log(FeO_X+MnO_X) - 0.82*\log(CaCO_3)$						
Model 2				0.40	19.6	0.37
FeO_X+MnO_X (deep)	0.99	0.35	0.015			
$\log(K_d) = 1.9 + 0.99*\log(FeO_X+MnO_X)$						